SAND2015-4611C

Proceedings of the ASME 2015 Power and Energy Conversion Conference
PowerEnergy2015
June 28-July 2, 2015, San Diego, California

PowerEnergy2015-49810

DRAFT: THERMODYNAMIC INVESTIGATION OF CONCENTRATING SOLAR POWER WITH THERMOCHEMICAL STORAGE

Brandon T. Gorman
Arizona State University
Tempe, Arizona, USA

Nathan G. Johnson*
Arizona State University
Mesa, Arizona, USA

James E. Miller
Sandia National Laboratories
Albuquerque, New Mexico, USA

Ellen B. Stechel
Arizona State University
Tempe, Arizona, USA

*Corresponding author: nathanjohnson@asu.edu, 1-480-727-5271

ABSTRACT

Concentrating solar power systems coupled to energy storage schemes, e.g. storage of sensible energy in a heat transfer fluid, are attractive options to reduce the transient effects of clouding on solar power output and to provide power after sunset and before sunrise. Common heat transfer fluids used to capture heat in a solar receiver include steam, oil, molten salt, and air. These high temperature fluids can be stored so that electric power can be produced on demand, limited primarily by the size of the capacity and the energy density of the storage mechanism. Phase changing fluids can increase the amount of stored energy relative to non-phase changing fluids due to the heat of vaporization or the heat of fusion. Reversible chemical reactions can also store heat; an endothermic reaction captures the heat, the chemical products are stored, and an exothermic reaction later releases the heat and returns the chemical compound to its initial state. Ongoing research is investigating the scientific and commercial potential of such reaction cycles with, for example, reduction (endothermic) and re-oxidation (exothermic) of metal oxide particles. This study includes thermodynamic analyses and considerations for component sizing of concentrating solar power towers with redox active metal oxide based thermochemical storage to reach target electrical output capacities of 0.1 MW to 100 MW. System-wide analyses here use one-dimensional energy and mass balances for the solar field, solar receiver reduction reactor, hot reduced particle storage, re-oxidizer reactor, power block, cold particle storage, and other components pertinent to the design. This work is part of a US Department of Energy (DOE) SunShot project entitled High Performance Reduction Oxidation of Metal Oxides for Thermochemical Energy Storage (PROMOTES).

INTRODUCTION

Renewable energy generation is expected to double over the next 25 years, with much of that growth coming from solar and wind generation (EIA 2014). Leading solar power generating technologies include solar photovoltaics (PV) and concentrating solar power (CSP). Solar PV markets have experienced rapid growth in residential, commercial, industrial, and utility markets due to recent reductions in hardware costs (Ardani 2014). Utilities have also turned to large-scale CSP systems for electricity generation in areas with high amounts of direct solar radiation (Mendelsohn et al. 2012, U.S. Department of Energy 2014a).

CSP systems include three or four major subsystems: the solar field for collecting and concentrating solar energy, a solar receiver for converting radiation to thermal energy, a power island for converting thermal energy into electrical power, and an optional thermal energy storage system to provide capacity conditions when the sun is not shining. Solar field designs include power towers, troughs, linear fresnel, and parabolic dish-engines, with U.S. amongst the leaders in power tower operation and future outlook (CSP World 2012). Power islands installed to date commonly include a steam turbine, with newly installed systems and ongoing research looking to gas turbines

Sandia National Laboratories is a multi-mission laboratory managed and operated by Sandia Corporation, a wholly owned subsidiary of Lockheed Martin Corporation, for the U.S. Department of Energy's National Nuclear Security Administration under contract DE-AC04-94AL85000

and combined-cycles for power generation (Mendelsohn et al. 2012). Although storage is not necessary in a CSP system, storage does provide several advantages by smoothing changes in power output during intermittent cloud disruptions and extending the system operational period for several hours after sunset or before the sunrise. These technical advantages over solar PV allow utilities to plan and schedule solar-storage systems similar to traditional dispatchable generation (Denholm and Hummon 2012). Storage is particularly useful as utilities seek options to avoid potential "duck curve" or "duck chart" behavior in the system load profile that can occur when solar PV power output declines in the late afternoon and residential loads increase as people arrive home from work or school (California ISO 2013).

BACKGROUND

Heat transfer fluids (HTFs) absorb energy in the solar receiver and release energy either directly or indirectly (through another HTF) into the power island to generate electricity. The mode of heat transfer may incorporate a change in sensible energy, latent heat due to a phase change, or chemical energy from a thermochemical reaction.

Common heat transfer fluids such as steam, oil, and molten salt capture (and transfer) sensible energy through a corresponding rise in temperature. Molten nitrate salt is the most common HTF with thermal stability as a liquid in the temperature range of 220°C to 565°C (Glatzmaier 2011). Molten salts are commonly used in power tower CSP systems whereas synthetic oils are commonly used in most linear concentrator trough CSP systems (Baharoon et al. 2015). Molten salts and oils are replacing steam as the HTF due to superior heat transfer capabilities and energy storage capacity. There can be several fluids used in a single CSP system—e.g., heat transfer fluid in the solar field (oil), thermal energy storage material (molten salt), and working fluid in the power island (steam) (Glatzmaier 2011).

Phase changing materials with both sensible heat and latent heat enthalpies offer improved energy density over counterpart fluids with only sensible heat enthalpy change. The generally low thermal conductivity of the solid phase poses a challenge during power discharge, however, and the poor power density of such materials offsets the benefit of high energy density. This makes phase changing materials an unlikely alternative to oil and molten salt in power tower and linear concentrator systems. Dish-engine systems may use phase changing materials as the HTF since heat transfer to the engine occurs at constant temperature (Shabgard et al. 2014, Sharifi et al. 2015).

Reversible thermochemical reactions can also be used as a mode of heat transfer that begins with an endothermic chemical reaction collecting heat from the sun, an optional step of storing the products, and concludes with an exothermic chemical reaction to transfer heat into the power block. Sensible heat exchange also occurs, though it can be small relative to the thermochemical reaction. Ongoing research is investigating the scientific and commercial potential of such reactions using reduced metal -oxide particles (Pardo et al. 2014, Wong 2011, Neises et al. 2012). In this program we are examining redox-active metal oxides that are mixed ionic-electronic conductors (MIEC). The MIEC metal oxides have specific attributes advantageous for use in thermochemical energy storage, which include:

- Rapid utilization of the bulk materials—Fast oxygen ion transport facilitates rapid and complete utilization—the reaction is not surface limited.
- Capability to reach higher temperatures—Metal oxides are stable at higher temperatures than oil and molten salt, and thereby can increase CSP system efficiency.
- High energy density in storage—Stored energy in the chemical reaction has the potential to far exceed stored energy in sensible-only or phase changing materials.
- Stability over a large number of cycles—The characteristics of mixed-ionic-electronic conductors allow manipulation of thermophysical parameters that influence their redox kinetics and operating temperatures, while resisting redox attrition over life-cycle of plant operation.
- Use of air gas turbine in the power block—Metal oxides can release heat through an exothermic re-oxidation reaction by interacting with air in an open gas turbine system. An additional advantage of the air gas power cycle is that it permits easy hybridization, for example with natural gas firing to continue power production after storage has been fully discharged.

Stoichiometry of the metal oxide redox reaction is simple, and produces only oxygen gas as a bi-product. Since some metal oxides remain solid at temperatures exceeding 1400°C, plant design is relatively simple requiring only radiation-solid and a solid-gas interfaces. A generalized equation for the metal oxide (in this case a perovskite MIEC) thermochemical energy storage and reduction extent (∂) is (McDaniel et al. 2013):

$$\mathrm{ABO_3} \leftrightarrow \mathrm{ABO_{3-\partial}} + \frac{\partial}{2}\mathrm{O_2(g)} \tag{1}$$

Reduction extent for the above reaction can physically range from 0 to 3. At 0 there is no oxygen produced, and at 3 the entirety of the reactant is consumed to produce the maximum amount of oxygen that is possible.

The SunShot Initiative and Thermal Energy Storage

One of the primary goals of the U.S. Department of Energy (DOE) SunShot Initiative is to reduce the levelized cost of electricity generated by CSP systems to at or below $0.06/kWh, without subsidy, by the year 2020 (U.S. Department of Energy 2014b). Storage will play a vital role in achieving this goal, as storage increases the utilization factor of the power system. DOE specifies several storage related targets, such as energy storage capacity > six hours, high exergetic efficiency (which exceeds 95% for low energy density systems), cost < $15/kWh$_{th}$, improved heat transfer and thermal energy storage media, and material degradation due to corrosion to < 15 μm/year (U.S. Department of Energy 2014c). The SunShot initiative has funded several awards for developing

thermochemical energy storage through its CSP: ELEMENTS program. The work presented in this study provides some early analyses from the project High Performance Reduction Oxidation of Metal Oxides for Thermochemical Energy Storage (PROMOTES) funded by the CSP: ELEMENTS program (U.S. Department of Energy 2014d). The PROMOTES project focuses on research and development of thermochemical energy storage (TCES) with metal oxide particles as the heat transfer media that undergo a reversible reduction-re-oxidation reaction to capture, store, and release heat. Materials development, direct integration with an air Brayton power cycle, reactor design, system design, and on-sun testing are key features of the project. The multi-faceted innovations sought by the award are examined in aggregate with system-wide technical and economic investigations introduced in this and other forthcoming studies.

There are three key performance targets the following PROMOTES system design and modeling seeks to evaluate within a subsystem boundary. This subsystem boundary begins from the metal oxide particles exiting the solar receiver reduction reactor and ends at the air exiting the re-oxidation reactor components depicted in Figs. 1 and 2. The performance targets are as follows:

1. Energetic efficiency ≥ 96%.
2. Exergetic efficiency ≥ 83%.
3. Thermal storage cost < \$15/kWh$_{th}$.

MODEL SETUP

This study uses custom models designed in Engineering Equation Solver (EES) and Matlab to complete thermodynamic investigations of TCES systems not represented in existing simulation packages. The EES and Matlab models facilitate exploratory research and design-driven analyses by allowing various input and output variables such as direct normal irradiance (DNI), storage capacity, extent of reduction of the metal oxide, storage size, gas turbine design configurations and states, and other component sizes and characteristics. Model results and analyses seek to size components, bound component-level parameters and states, and conduct thermodynamic "negotiation" between components to meet system-level performance targets. Initial analyses for a 100 kW$_e$ simple cycle air Brayton power block are described here. The 100 kW$_e$ system serves as a reference case for discussion and future research for system capacities up to 100 MW$_e$.

System Description

A diagram of components in the PROMOTES system is given in Fig. 1 (U.S. Department of Energy 2014e). The five major components modeled in this study are within the system boundary of Fig. 2.

- Solar Receiver Reduction Reactor (SR3): Receives solar flux from the solar field to heat and reduce (to a reduction extent of ∂) the metal oxide media (ABO_3 to $ABO_{3-\partial}$) through the endothermic reaction Eq. 1.
- Hot Storage (HS): Thermal storage for the hot, reduced metal oxide media that is charged (filled) during sunlight hours and discharged (emptied) during the hours from sunset to sunrise.
- Re-Oxidation Reactor (ROx): Mixes hot reduced metal oxide media with pressurized air to create an exothermic reaction resulting in high-temperature air that enters the air Brayton engine for power generation.
- Cold Storage (CS): Storage for the cold, oxidized metal oxide media that is charged (filled) and discharged (emptied) as hot storage is emptied and filled, respectively.
- Heat Exchanger (HX): Recovers heat from oxygen exiting the SR3 to preheat metal oxide discharged from cold storage.

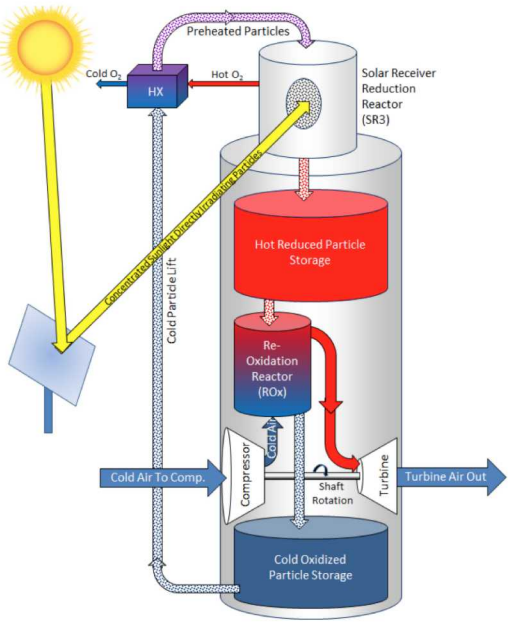

Fig. 1 Component diagram of the PROMOTES system. (U.S. Department of Energy 2014e)

A 1-D steady state quasi-equilibrium model was also developed for the Brayton cycle to calculate required state information residing outside of the system boundary to determine necessary state conditions for the air mass leaving the ROx reactor. The EES model specifies pressure, temperature, and mass flow for the air leaving the ROx reactor based upon manufacturer reported values for power cycle output, efficiency, air flow rate, and temperatures at other points in the Brayton power block subsystem. The state information for temperature and mass flow rate of air is then input into the larger PROMOTES thermodynamic model written in Matlab.

Quasi-Steady State Thermodynamic Modeling

Quasi-steady state modeling is based upon the diagram in Fig. 2 comprised of 21 states. Each of the states, including those outside the system boundary, are required for energy balance equations about each of the five major components introduced above.

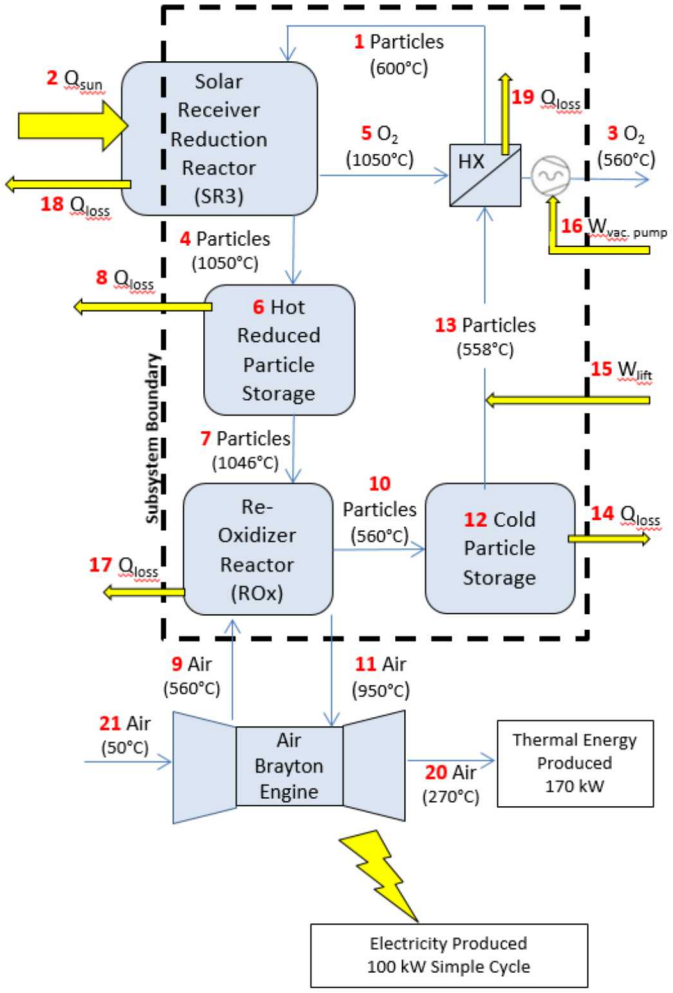

Fig. 2 Schematic of the PROMOTES system showing system flows currently considered in the model. (U.S. Department of Energy 2014e)

SR3: Five pertinent energy flows around the SR3 in Eq. 2 include the inlet metal oxide molar flow (State 1), the outlet metal oxide molar flow (State 4), the outlet oxygen flow (State 5), the incoming concentrated solar flux (State2), and heat loss (State 18). Subscripts in Eq. 2 and the remaining equations pertain to states numbers given in Fig. 2. The molar flow rate of metal oxide particles ($[\dot{n}_{ABO_3}]$ is abbreviated across States 1, 4, and 13 ($[\dot{n}_{ABO_3}]_{1,4,13}$) and across states 7 and 10 ($[\dot{n}_{ABO_3}]_{7,10}$) because they are equivalent across states in the simplified nomenclature. The ambient temperature is denoted as T_0. The stored chemical energy of the redox reaction is the enthalpy of reduction (and oxidation) per mole of oxygen gas, denoted as H_{red}. Sensible energy is tracked across temperature changes using the specific heat capacity of the metal oxide particles and oxygen denoted as $\bar{C}_{p,ABO_3}$ and $\bar{C}_{p,O_2}$, respectively.

$$\begin{aligned}\Delta E_{SR3} = 0 &= \dot{Q}_2 - \dot{Q}_{18} \\ &+[\dot{n}_{ABO_3}]_{1,4,13} \cdot \bar{C}_{p,ABO_3} \cdot (T_1 - T_4) \\ &-[\dot{n}_{ABO_3}]_{1,4,13} \cdot \frac{\partial}{2} \cdot H_{red} \\ &-[\dot{n}_{O_2}]_5 \cdot \bar{C}_{p,O_2} \cdot (T_5 - T_0)\end{aligned} \tag{2}$$

Hot Storage: Four pertinent energy flows in Eq. 3 around the hot reduced particle storage include the inlet metal oxide molar flow (State 4), the outlet metal oxide molar flow (State 7), heat loss (State 8), and the stored metal oxide (HS or State 6). The inlet metal oxide molar flow is determined by the flow rate of the SR3 and the outlet metal oxide molar flow is determined by the flow rate of the ROx Reactor. Heat loss is taken as a function of the amount of stored sensible heat and time.

$$E_{HS}^{t} = E_{HS}^{t-1} + \dot{E}_4^{t-1} - \dot{E}_7^{t-1} - \dot{Q}_8^{t-1} \tag{3}$$

ROx reactor: Five pertinent energy flows in Eq. 4 around the ROx reactor include the inlet metal oxide molar flow (State 7), the outlet metal oxide molar flow (State 10), the inlet air flow (State 9), the outlet air flow (State 11), and heat loss (State 17). Outlet air flow properties such as temperature and mass flow rate are fixed to meet specifications of the air Brayton engine make and model. The current equation set assumes that both the pressure drop and air mass decrease across the ROx is negligible, which will be revisited and refined in future work.

$$\begin{aligned}\Delta E_{ROx} = 0 &= \left[\dot{n}_{air}\right]_{9,11} \cdot \bar{C}_{p,air} \cdot (T_9 - T_{11}) \\ &+[\dot{n}_{ABO_3}]_{7,10} \cdot \bar{C}_{p,ABO_3} \cdot (T_7 - T_{10}) \\ &+[\dot{n}_{ABO_3}]_{7,10} \cdot \frac{\partial}{2} \cdot H_{red} \\ &-\dot{Q}_{17}\end{aligned} \tag{4}$$

Cold Storage: Four pertinent energy flows in Eq. 5 around the cold oxidized particle storage include the inlet metal oxide molar flow (State 10), the outlet metal oxide molar flow (State 13), heat loss (State 14), and the stored metal oxide (CS or State 12). The inlet metal oxide molar flow is determined by the flow rate of the ROx reactor and the outlet metal oxide particle flow rate is determined by the flow rate of the SR3. Heat loss is taken as a function of the amount of stored sensible heat and time.

$$E_{CS}^{t} = E_{CS}^{t-1} + \dot{E}_{10}^{t-1} - \dot{E}_{13}^{t-1} - \dot{Q}_{14}^{t-1} \tag{5}$$

HX: Five pertinent energy flows in Eq. 6 around the heat exchanger include the inlet metal oxide molar flow (State 13), the outlet metal oxide molar flow (State 1), the inlet oxygen molar flow (State 5), the outlet oxygen molar flow (State 3), and heat loss (State 19). The equation uses the number of transfer units method to calculate the effectiveness of a counter-current flow heat exchanger, then heat loss is taken as a function of effectiveness.

$$\begin{aligned}\Delta E_{HX} = 0 = [\dot{n}_{O_2}]_5 \cdot \bar{C}_{p,O_2} \cdot (T_5 - T_3) \\ +[\dot{n}_{ABO_3}]_{1,4,13} \cdot \bar{C}_{p,ABO_3} \cdot (T_{13} - T_1) \\ -\dot{Q}_{19}\end{aligned} \quad (6)$$

Work: The work terms are considered parasitic losses that are not used in energy balance equations around the components, however, their effect is on the total subsystem efficiency. One pertinent energy flow in Eq. 7 for the lift uses the metal oxide molar mass to convert molar flow (State 13) to mass flow which is denoted as $\dot{m}_{ABO_3}^{1,4,13}$. The conversion is used with input parameters to calculate the net energy flow requirements of the lift.

$$\dot{W}_{15,lift} = \dot{m}_{ABO_3}^{1,4,13} \cdot c_{lift} \cdot h_{lift} / \eta_{lift} \quad (7)$$

There is one pertinent energy flow in Eq. 8 for the O_2 vacuum pump which is the oxygen molar flow (State 5). The net energy flow requirements of the vacuum pump are calculated by also using the universal gas constant, pressure, and efficiency term. Further work will be done by including an equation for sweep gas to compare performance and economics to the vacuum pump.

$$\dot{W}_{16,pump} = [\dot{n}_{O_2}]_5 \cdot R \cdot T_0 \cdot \ln(\frac{P_0}{P_{O_2}}) / \eta_{pump} \quad (8)$$

The energy balance equation about each component is used in a systems of equations for quasi-steady state thermodynamic evaluation of the full PROMOTES system. Computation begins by selecting static input values (parameters and sensitivity variables) for the simulation and continues with hourly quasi-steady state simulations that model performance during changing conditions of a single day or multiple days:

1. Calculate the solar flux into the receiver $\dot{Q}_2$ based on solar field area, DNI (only when greater than 350 W/m^2, otherwise particles do not flow), and optical efficiencies.
2. Calculate the molar flow rates of the particles, $[\dot{n}_{ABO_3}]_{1,4,13}$, using SR3 Eq. 2. The metal oxide's properties of specific heat, enthalpy of reduction, and ∂ affect flow rate. The molar flow rate of the oxygen, $[\dot{n}_{O_2}]_5$, is then calculated and depends on ∂ and $[\dot{n}_{ABO_3}]_{1,4,13}$.
3. According to the specified dispatch schedule, calculate the required molar flow rate of particles, $[\dot{n}_{ABO_3}]_{7,10}$, using ROx Eq. 4.
4. Use $[\dot{n}_{ABO_3}]_{1,4,13}$ and $[\dot{n}_{ABO_3}]_{7,10}$ to charge (fill) and discharge (empty), respectively, the hot reduced particle storage in Eq. 3. The stored particles are subject to a modest temperature drop during residence time.
5. Use $[\dot{n}_{ABO_3}]_{7,10}$ and $[\dot{n}_{ABO_3}]_{1,4,13}$ to charge (fill) and discharge (empty), respectively, the cold oxidized storage in Eq. 5. The stored particles are subject to a modest temperature drop during residence time.
6. Use heat content of $[\dot{n}_{O_2}]_5$ in Eq. 6 to pre-heat the particles in the heat exchanger. The heat exchanger is subject to realistic efficiency losses.
7. Account for the work and parasitic terms, namely lift efficiency, vacuum pumping (Ermanoski et al. 2013) or sweep gas to control the partial pressure of O_2.
8. The net energy entering reduced storage and entering the air Brayton engine is used to calculate energetic and exergetic efficiencies of the thermal storage subsystem boundary.

Input Data

The enthalpy of reduction varies as a function of reduction extent, seen in Eq. 9. This quadratic equation is fitted for the range from $\partial = 0.2$ to $\partial = 0.5$ and outputs units in kJ/mol-O_2. As reduction extent increases, the amount of stored chemical energy increases.

$$H_{red}(\partial) = 147.5 + 1057 \cdot \partial + 633 \cdot \partial^2 \quad (9)$$

Table 1 below lists input data and parameters used for subsequent results, analysis, and discussion. These are representative and will be refined in future work and subjected to sensitivity and parameter screens. Many of these parameters will be used in thermodynamic "negotiation" to achieve system-level performance targets. It is evident that an increased rate of heat loss from the storage units will require reduced heat losses in the Re-Oxidizer reactor. It is also apparent that a lower heat of reduction implies an increased flow rate of particles to generate the same amount of energy in storage to maintain six hours of power generation after sunset—i.e., increased costs. This model will eventually scale up to 100 MW_e, which brings into consideration cases like power block efficiency for larger system sizes. In this case the power block expenses a large amount of unused thermal energy as it runs in a single cycle configuration. Tower height is taken from the height of existing AORA Solar Tulip Power Tower that is rated at 100 kW_e.

Table 1 Input values and parameters for simulated 100 kW_e system for the purposes here.

Component	Variable	Value
	(R) Gas constant	8.314 J/ mol×K
	(P_0) Ambient pressure	101325 Pa
Metal oxide	Molar mass	0.1416 kg/mol
	($\bar{C}_{p,ABO_3}$) Specific heat	124.7 J/mol×K (15 R)
	(∂) Reduction extent	0.2 to 0.5
Oxygen	($\bar{C}_{p,O_2}$) Specific heat	29.10 J/ mol×K (7/2 R)
Solar field	Area	832 m^2
	Efficiency	60%
Receiver	Aperture area	0.264 m^2
	Emissivity	0.9
	Additional Q_{loss}	$(Q_2 - Q_{loss}^{re-radiation}) \cdot 0.05$
	T1	~250 °C
	T4	1050 °C
	(P_{O_2}) Partial pressure of O_2	1000 Pa
Storage	Heat loss rate	1% per day
Re-Oxidizer	Energy loss	1% of incoming energy
	T11	950 °C
Power block	Electrical efficiency	30%
	Thermal efficiency	50%
Work terms	(c_{lift})*	10.813 m/s^2
	(h_{lift}) Tower height	35 m
	(η_{lift})* Efficiency	80%
	(η_{pump})** Efficiency	40%

*(de la Vergne J. 2003) **(Ermanoski et al. 2013)

The net solar flux into the receiver aperture ($\dot{Q}_2$) is dependent upon the size of the solar field (area), solar field efficiency which includes mirror efficiency, cosine losses, attenuation, etc. of beam radiation, hourly DNI values, minus re-radiation heat loss (based on T4 and aperture area). Solar field efficiency and additional heat loss values are constant and representative for simplicity, and will be expanded upon in future models of end-to-end efficiency. DNI data is selected from different days of the year to represent low, medium, and high solar insolation. DNI data is taken from Phoenix, AZ Sky Harbor International Airport (National Renewable Energy Laboratory 1991-2005).

The solar multiple is defined as the ratio of the solar field's capacity to the power block's capacity. Without an optimal solar multiple, either the solar field or the power block is underutilized. For the purposes here, the solar multiple is not used to optimize plant operation. The solar field area is fixed as seen in Table 1.

A simple air Brayton power cycle with one recuperation loop is used for the 100 kW_e reference system here. Larger systems approaching 100 MW_e will implement a combined cycle power block with aid of a bottoming Rankine cycle. The electrical efficiency of the power block increases as the size of the plant design increases. Power block efficiency values are taken from specification sheets provided by manufacturer reference material and primary and secondary sources that compile technical data of commercial gas turbines (Turbomachinery Handbook 2015, Power Engineering International 2012).

RESULTS AND ANALYSIS

Every value of ∂ requires a different metal oxide molar flow from the Hot Storage to the ROx reactor to run the power block and a different sized Hot Storage to achieve six hours of off-sun power generation. The lowest reduction extent considered (∂ = 0.2) requires 4.011 mol/s of metal-oxide flow from the Hot Storage bin to the ROx reactor. The requisite size of storage can be calculated as 50,583 m^3 by using a metal oxide molar volume (0.345 m^3/mol), a packing density (0.65), a specified amount of storage (six hours) with contingency or ullage space (10%), and a rated power output (100 kW_e) and electrical efficiency (30%) of the power block. At the highest reduction extent considered (∂ = 0.5), identical parameters require 1.957 mol/s of metal oxide flow from the Hot Storage bin to the ROx reactor and occupies 24,680 m^3, or approximately 48.8% of the flow and storage size needed for the lowest reduction extent considered.

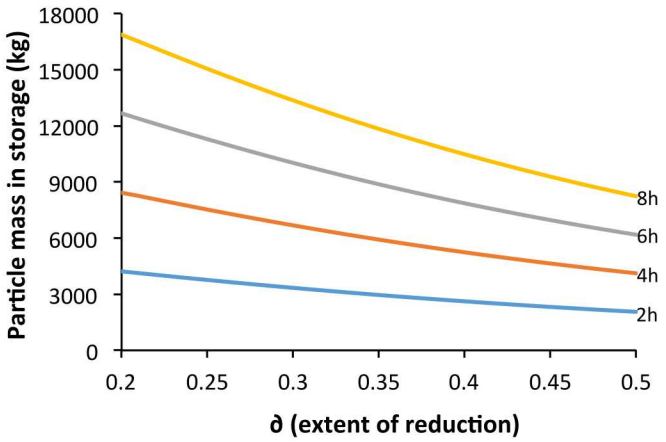

Fig. 3 Extent of reduction effects the amount of particles to hit off-sun power targets. Assumes 100% SR3 outlet to air Brayton engine inlet efficiency.

Varying the storage performance target depicted in Fig. 3 demonstrates that the amount of metal oxide particle mass to hit off-sun thermal energy storage targets is inversely related to the extent of reduction—i.e., as extent of reduction increases, required particle mass in storage decreases. For the SunShot Initiative's target of six hours, Table 1's predefined inputs and parameters results in more than 12,000 kg of metal oxide particles at $\partial = 0.2$ and drops to slightly more than 6,000 kg of metal oxide particles at $\partial = 0.5$. Using the model inputs from Table 2, the target of 1500 kJ/kg is not met for a system operating with the currently simulated parameters. The energy density goes from 597 kJ/kg at $\partial = 0.2$ to 1213 kJ/kg at $\partial = 0.5$.

Table 2 Particle energy density (kJ/kg) with paired T_{high} and T_{low} values when $\partial = 0.5$.

		T_{high}			
		1050 °C	1100 °C	1150 °C	1200 °C
T_{low}	200 °C	**1520**	**1563**	**1606**	**1648**
	300 °C	1435	1478	**1520**	**1563**
	400 °C	1350	1392	1435	1478
	500 °C	1264	1307	1350	1392
	600 °C	1179	1222	1264	1307

Table 2 is an assorted list of paired T_{high} and T_{low} to consolidate the energy density of the thermochemical particles at various operating conditions. The current simulation sets T_{high} = 1050 °C and T_{low} = 560°C, yet does not achieve the desired energy density target of 1500 kJ/kg. We can see that by lowering T_{low} or raising T_{high} 1500 kJ/kg is possible (bold values in Table 2)—i.e, via increased sensible energy storage.

Three representative days were considered to demonstrate variations in 100 kW_e power tower operation in changing solar radiation: high solar radiation at the summer solstice in June, medium solar radiation around the spring equinox in April, and low solar radiation at the winter solstice in December.

Fig. 4 shows the particle flow rate through the receiver to hot storage as a function of DNI and ∂. The peak metal oxide flow rate decreased from approximately 4.20 mol/s at the lowest reduction extent considered, $\partial = 0.2$, to approximately 2.00 mol/s at the highest reduction extent considered, $\partial = 0.5$, during the summer solstice, which has one of the highest amount of daily irradiation throughout the year. In contrast, at the opposite extreme during the winter solstice, the peak particle flow rate is reduced to approximately 3.50 mol/s at the lowest extent considered, and approximately 1.70 mol/s at the highest reduction extent considered (Fig. 5.) Future work will have to optimize the solar multiple so that ideal plant operation can be maintained throughout the year.

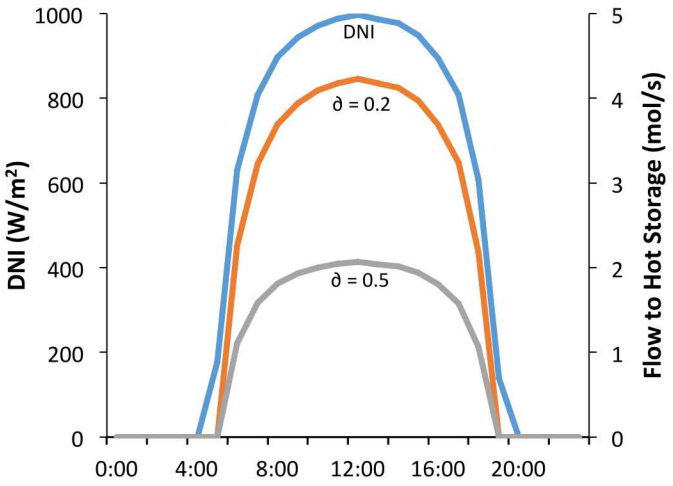

Fig. 4 Particle flow rate varies with extent of reduction (∂) for the Summer solstice on June 10, 1986.

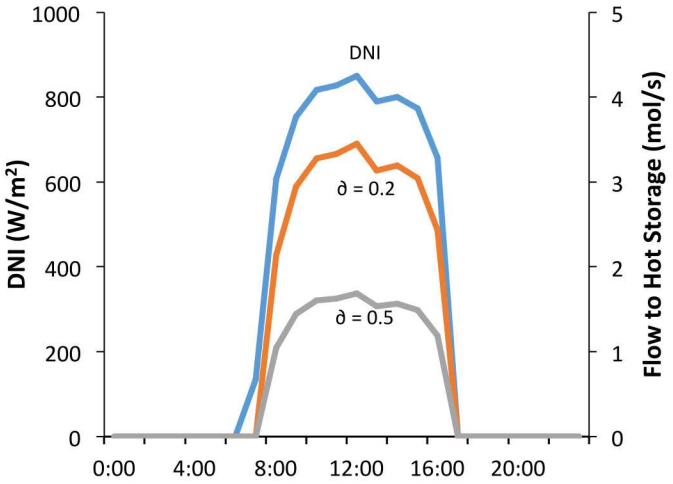

Fig. 5 Metal oxide molar flow rate varies with extent of reduction (∂) for the Winter solstice on December 16, 2001.

Table 3 translates Figs. 4 and 5 metal oxide flow rate information into daily system operating time at full power. The lower flow rate in December for $\partial = 0.2$ is reflected in a lower aggregate amount of material reduced per day, which lowers daily operating time. Sensitivity analyses on day of the year and extent of reduction provides valuable information on targeting six hours of off-sun thermal energy storage when facing low solar irradiation seen in December and high solar irradiation in June. As a consequence of six hours of off-sun operation, on-sun operation varies from one to six hours depending on solar insolation seen in Table 3, with the fixed and non-optimized solar multiplier used here.

Table 3 System operation over selected times of year and extent of reduction (∂).

	June (High solar)	
Irradiation (Wh/m^{2}day)	11,778	
Extent of reduction	$\partial = 0.2$	$\partial = 0.5$
Particles reduced (mol/day)	169,254	82,769
Operating time* (hr/day)	11.72	11.75
	April (Medium solar)	
Irradiation (Wh/m^{2}day)	9,328	
Extent of reduction	$\partial = 0.2$	$\partial = 0.5$
Particles reduced (mol/day)	130,875	64,051
Operating time* (hr/day)	9.06	9.09
	December (Low solar)	
Irradiation (Wh/m^{2}day)	7,013	
Extent of reduction	$\partial = 0.2$	$\partial = 0.5$
Particles reduced (mol/day)	96,974	47,480
Operating time* (hr/day)	6.72	6.74

Assumes 100% SR3 outlet to air Brayton engine inlet efficiency. * Operating time is the number of hours that the system can generate power given the selected day's solar insolation—i.e., on-sun hours + off-sun hours. Six hours of storage is possible in all cases, however, the number of power generating hours during sunlight hours varies.

Energetic efficiency of the predefined PROMOTES subsystem boundary (between the SR3 and gas turbine) is defined in Eq. 10. The energy in State 11 is the net energy into the air Brayton engine, State 4 is the energy moving from the SR3 into hot storage, State 9 is the energy moving from the air Brayton (compressor) into the ROx reactor, State 10 is energy recirculated within the system that is not transferred into the air through the exothermic reaction of air and particles, and HS is the unused energy remaining in Hot Storage. The hour of operation is denoted as t and the number of hours of operation is denoted as m. The value of t is equal to 1 for the hour Hot Storage begins charging (filling) in the day time, and t is equal to m for an hour between sunset and the next day's sunrise. If Hot Storage is completely discharged (emptied) then $E_{HS}^{m} = 0$.

$$\eta_{\text{energy}} = \frac{E_{HS}^{m} + \sum_{t=1}^{m} \dot{E}_{11}^{t}}{\sum_{t=1}^{m} \dot{E}_{4}^{t} + \dot{E}_{9}^{t} - \dot{E}_{10}^{t}} \qquad (10)$$

According to the predefined PROMOTES subsystem boundary, Eq. 10 results in an energetic efficiency of 98.78% for $\partial = 0.5$, exceeding the performance target. Alternatively, the total subsystem energetic efficiency is 85.78% for $\partial = 0.5$ when incorporating subsystem-wide heat and parasitic losses (work). These calculations are based upon the several assumed input values in Table 1 that will be further explored using sensitivity analysis to bound the input-output parameters of detailed component-level models.

DISCUSSION

This study on MIEC metal oxides for thermochemical energy storage aims to characterize the thermodynamic performance and cost constraints that affect plant design. Using a detailed model of subsystem operating conditions, optimal system parameters can be used to increase subsystem efficiency (and total system efficiency). According to Falcone's (1986) study on a 100MW$_e$ external molten salt power tower, system-wide annual fractional energy losses from incident radiation on heliostat field (1,397 GWh$_{th}$) to the net electrical energy onto the grid (202 GWh$_e$) have been reported to be as large as 85.5%, which includes the thermal-to-electric fractional energy loss of 58.2%. The losses in thermal-to-electric conversion can be reduced by increasing turbine inlet temperature and adding a bottoming Rankine cycle (combined cycle system)—common in larger capacity power blocks. The high-temperature gases resulting from the exothermic reaction with MIEC metal oxides facilitates this efficiency gain.

Plant designs will vary for systems sized from 100 kW$_e$ to 100 MW$_e$. Air Brayton engine specifications will have increased efficiencies as power block size increases; large commercial gas turbines increase efficiency by using greater air pressure ratios and higher turbine inlet temperatures. Larger plants will also utilize the combined cycle system, where exhaust heat from the air Brayton engine is sent to a bottoming Rankine cycle. Expected turbine inlet temperatures can range between 900 ºC to 1400 ºC.

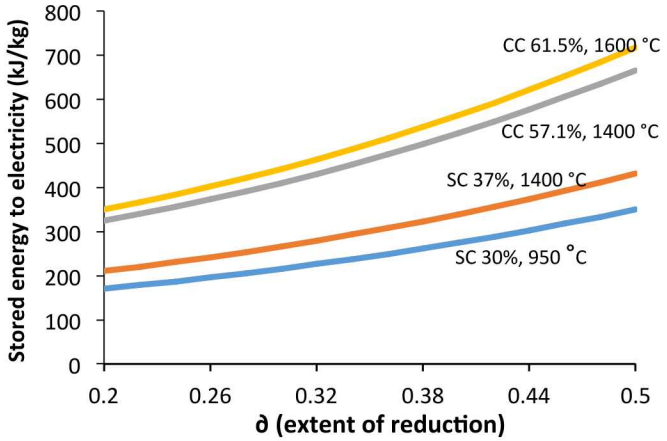

Fig. 6 Power block efficiency limits the amount of thermal energy converted into electricity. Data retrieved from Turbomachinery Handbook (2015) and Power Engineering International (2012). Assumes 100% SR3 outlet to air Brayton engine inlet efficiency.

Fig. 6 demonstrates the increase in thermal energy to electrical energy conversion when using higher efficiency power blocks from higher temperatures and larger combined

cycle systems. The drop from Fig. 3 thermal energy density is due to inefficiencies in the power block. Single cycle (SC) are for smaller plant designs, while combined cycle (CC) are for larger designs. Combined cycles can increase the thermal-to-electric efficiency of the power block, with a 1400 ºC turbine inlet temperature, from 37% to 57.1%.

Increased flow rate of reduced metal oxides to hot reduced storage will increase plant operating time if storage capacity permits. Factors that can reduce heat losses in the receiver (more energy to reduce the inlet metal oxide molar flow of the SR3), increase effectiveness of the heat exchanger (the inlet metal oxide molar flow of the SR3 requires less sensible energy to hit State 4's temperature), and reduce temperature drops in cold storage (requires less energy to hit State 4's temperature) are some examples. The most direct method to increase operating time of the power tower is by increasing the solar multiple, however.

Future work will incorporate sensitivity analyses to identify the range of feasible input and output state parameters that meet both technical and economic metrics and provide guidance to component design. Models from this study will facilitate the combined techno-economic optimization and provide an opportunity for comparative analysis against non-metal oxide systems in the DOE's System Advisor Model.

ACKNOWLEDGEMENTS

The U.S. Department of Energy (DOE) SunShot Initiative provided funding for the project entitled High Performance Reduction/Oxidation Metal Oxides for Thermochemical Energy Storage (PROMOTES) under award number DE-FOA-0000805-1541 as part of the CSP:ELEMENTS program.

The authors would like to thank all the members of the PROMOTES team for useful conversations and insights, including Hany Al Ansari, Andrea Ambrosini, Sean Babinec, Eric Coker, Cliff Ho, Sheldon Jeter, Peter Loutzenheiser, and Andrew Shrader.

Sandia is a multiprogram laboratory operated by Sandia Corporation, a Lockheed Martin Company, for the United States Department of Energy's National Nuclear Security Administration under contract DE-AC04-94AL85000.

REFERENCES

[1] U.S. Energy Information Administration, 2014. Annual Energy Outlook. U.S. Energy Information Administration.

[2] Ardani, K., 2014. Benchmarking Non-Hardware Balance-of-System (Soft) Costs for US Photovoltaic Systems Using a Bottom-Up Approach and Installer Survey. National Renewable Energy Laboratory.

[3] Mendelsohn, M., Lowder, T., Canavan, B., 2012. Utility-Scale Concentrating Solar Power and Photovoltaics Projects: A Technology and Market Overview. National Renewable Energy Laboratory.

[4] U.S. Department of Energy, 2014a. "MAP: Concentrating Solar Power Across the Unites States", from http://energy.gov/articles/map-concentrating-solar-power-across-united-states, December 28, 2014.

[5] CSP World, 2012. "MAP: Concentrating Solar Power World Map", from http://www.csp-world.com/cspworldmap, January 9, 2015.

[6] Denholm, P., Hummon, M., 2012. Simulating the Value of Concentrating Solar Power with Thermal Energy Storage in a Production Cost Model. National Renewable Energy Laboratory.

[7] California ISO, 2013. "What the Duck Curve Tells us About Managing a Green Grid", http://www.caiso.com/Documents/FlexibleResourcesHelp Renewables_FastFacts.pdf, December 28, 2014.

[8] Glatzmaier, G., 2011. Summary Report for Concentrating Solar Power Thermal Storage Workshop: New Concepts and Materials for Thermal Energy Storage and Heat-Transfer Fluids. National Renewable Energy Laboratory.

[9] Baharoon, D. A., Rahman, H. A., Omar, W. Z. W., & Fadhl, S. O., "Historical development of concentrating solar power technologies to generate clean electricity efficiently–A review." *Renewable and Sustainable Energy Reviews*, **2015**, *41*, 996-1027.

[10] Shabgard, H., Faghri, A., Bergman, T. L., & Andraka, C. E., "Numerical Simulation of Heat Pipe-Assisted Latent Heat Thermal Energy Storage Unit for Dish-Stirling Systems." *Journal of Solar Energy Engineering*, **2014**, *136*(2), 021025.

[11] Sharifi, N., Faghri, A., Bergman, T. L., & Andraka, C. E., "Simulation of heat pipe-assisted latent heat thermal energy storage with simultaneous charging and discharging." *International Journal of Heat and Mass Transfer*, **2015**, *80*, 170-179.

[12] Pardo, P., Deydier, A., Anxionnaz-Minvielle, Z., Rougé, S., Cabassud, M., & Cognet, P., "A review on high temperature thermochemical heat energy storage." *Renewable and Sustainable Energy Reviews*, **2014**, *32*, 591-610.

[13] Wong, B., *Thermochemical heat storage for concentrated solar power--thermochemical system reactor design for thermal energy storage*; DE-FG36-08GO18145; General Atomics: 2011.

[14] Neises, M.; Tescari, S.; de Oliveira, L.; Roeb, M.; Sattler, C.; Wong, B., "Solar-heated rotary kiln for thermochemical energy storage." *Sol. Energy*, **2012**, 86 (10), 3040.

[15] McDaniel, A. H.; Miller, E. C.; Arifin, D.; Ambrosini, A.; Coker, E. N.; O'Hayre, R.; Chueh, W. C.; Tong, J., "Sr- and Mn- doped LaAlO3-δ for solar thermochemical H2 and CO production." *Energy and Environmental Science*, **2013**, 6, 2424-2428.

[16] U.S. Department of Energy, 2014b. "Concentrating Solar Power", from http://energy.gov/eere/sunshot/concentrating-solar-power, December 28, 2014.

[17] U.S. Department of Energy, 2014c. "Thermal Storage Research and Development for CSP Systems", from http://energy.gov/eere/sunshot/thermal-storage-rd-csp-systems, December 28, 2014.

[18] U.S. Department of Energy, 2014d. "Project Profile: High Performance Reduction/Oxidation Metal Oxides for

Thermochemical Energy Storage", from http://energy.gov/eere/sunshot/project-profile-high-performance-reductionoxidation-metal-oxides-thermochemical-energy, December 28, 2014.
[19] U.S. Department of Energy, 2014e. [System diagram of PROMOTES]. High Performance Reduction/Oxidation Metal Oxides for Thermochemical Energy Storage. Available from energy.gov/sites/prod/files/styles/large/public/SNL%20Webpage%20Picture_0.jpg, January 8, 2015.
[20] Ermanoski, I.; Siegel, N. P.; Stechel, E. B., "A New Reactor Concept for Efficient Solar-Thermochemical Fuel Production." *J. Solar Ener. Eng.* **2013,** *135* (3), 031002
[21] de la Vergne J., (2003). *Hard Rock Miner's Handbook, 3rd Ed.* McIntosh Engineering Limited. Tempe, AZ, 215.
[22] National Renewable Energy Laboratory (1991-2005). National Solar Radiation Data Base [722780TY.csv]. Retrieved from rredc.nrel.gov/solar/old_data/nsrdb/1991-2005/data/tmy3/722780TY.csv, November 2014.
[23] (2014) Electrical Generation Specifications. *Turbomachinery Handbook (2015),* 77-83.
[24] (2012) Gas Turbine Technical Data. *Power Engineering International (2012),* 34-42.
[25] Falcone, P. K., (1986). *A handbook for solar central receiver design* (No. SAND-86-8009). Sandia National Labs. Livermore, CA (USA).